Materials Science & Engineering C 120 (2021) 111720

Contents lists available at ScienceDirect

Materials Science & Engineering C

journal homepage: www.elsevier.com/locate/msec

Electrospun GelMA fibers and p(HEMA) matrix composite for corneal tissue engineering

Tugce A. Arica [a], Meltem Guzelgulgen [b], Ahu Arslan Yildiz [b], Mustafa M. Demir [a,*]

[a] Department of Material Science and Engineering, Izmir Institute of Technology, 35430 Izmir, Turkey
[b] Department of Bioengineering, Izmir Institute of Technology, 35430 Izmir, Turkey

ARTICLE INFO

Keywords:
Biomaterial
Cell adhesion and growth
Composites
Hydrogels
Protein adsorption

ABSTRACT

The development of biocompatible and transparent three-dimensional materials is desirable for corneal tissue engineering. Inspired from the cornea structure, gelatin methacryloyl-poly(2-hydroxymethyl methacrylate) (GelMA-p(HEMA)) composite hydrogel was fabricated. GelMA fibers were produced via electrospinning and covered with a thin layer of p(HEMA) in the presence of *N,N′*-methylenebisacrylamide (MBA) as cross-linker by drop-casting. The structure of resulting GelMA-p(HEMA) composite was characterized by spectrophotometry, microscopy, and swelling studies. Biocompatibility and biological properties of the both p(HEMA) and GelMA-p(HEMA) composite have been investigated by 3D cell culture, red blood cell hemolysis, and protein adsorption studies (i.e., human serum albumin, human immunoglobulin and egg white lysozyme). The optical transmittance of the GelMA-p(HEMA) composite was found to be approximately 70% at 550 nm. The GelMA-p(HEMA) composite was biocompatible with tear fluid proteins and convenient for cell adhesion and growth. Thus, as prepared hydrogel composite may find extensive applications in future for the development of corneal tissue engineering as well as preparation of stroma of the corneal material.

1. Introduction

Cornea, one of the avascular connective tissue present at the front of the eye, serves two important functions. It, first, keeps safe the eye from mechanical damage and infections and second, functions as a main optical component by refracting 70% of the incoming light [1,2]. The corneal stroma constitutes 90% of the thickness of the cornea and consists of aligned collagen fibrils (82% of the dry weight) [3]. They form triple-helix bundles with diameters of approximately 200–350 nm, which line up to form a flat lamellar sheet. The lamellar sheets of the stroma are layered on top of each other, and glycoproteins and keratin sulfate or chondroitin sulfate are located between fibrils along with other collagens and preserve the transparency of the cornea while keeping it hydrated [4]. Additionally, stroma provides many biochemical and biomechanical functions to the cornea including tensile strength and stability. Corneal disease is a leading cause of blindness, affecting 10 million people in the world [5,6]. Corneal transplantation from human donor tissue is a standard procedure for treating corneal diseases and restoring vision. However, the lack of donors has prompted scientists to explore alternative solutions. Poly(methyl methacrylate) is the first clinically successful synthetic polymeric material to be recommended for keratoprosthesis. However, such rigid and hydrophobic materials have been caused a variety of complications [7]. Therefore, research on the development of artificial corneas and biocompatible scaffolds has focused on hydrophilic soft materials that support surface cell adhesion [8–11].

In recent years, various synthetic or natural hydrogel materials have been used for corneal stroma tissue engineering studies in diverse forms and formulations due to their physical properties similar to soft tissues [8]. Among them, collagen and gelatin have been the mostly used natural materials in the fields of the tissue engineering. Gelatin is a protein and obtained by slow heat denaturation of collagen, during this process three-dimensional structure of the collagen gradually starts to unwind and converted into gelatin. The biomedical applications of gelatin are limited due to its poor thermostability and the undesired effect of the various bifunctional crosslinking agents on its biocompatibility [12]. Generally, semi-synthetic hydrogel from gelatin is synthesized by the reaction of amine groups of gelatins with methacrylic acid anhydride (GelMA). The double bonds in the GelMA structures raised from the incorporation of methacrylic acid are used for the preparation of GelMA hydrogel by free-radical polymerization in the presence of a photo-initiator. As reported earlier, the synthesized GelMA hydrogels have

* Corresponding author.
E-mail address: mdemir@iyte.edu.tr (M.M. Demir).

https://doi.org/10.1016/j.msec.2020.111720
Received 21 August 2020; Received in revised form 8 November 2020; Accepted 10 November 2020
Available online 13 November 2020

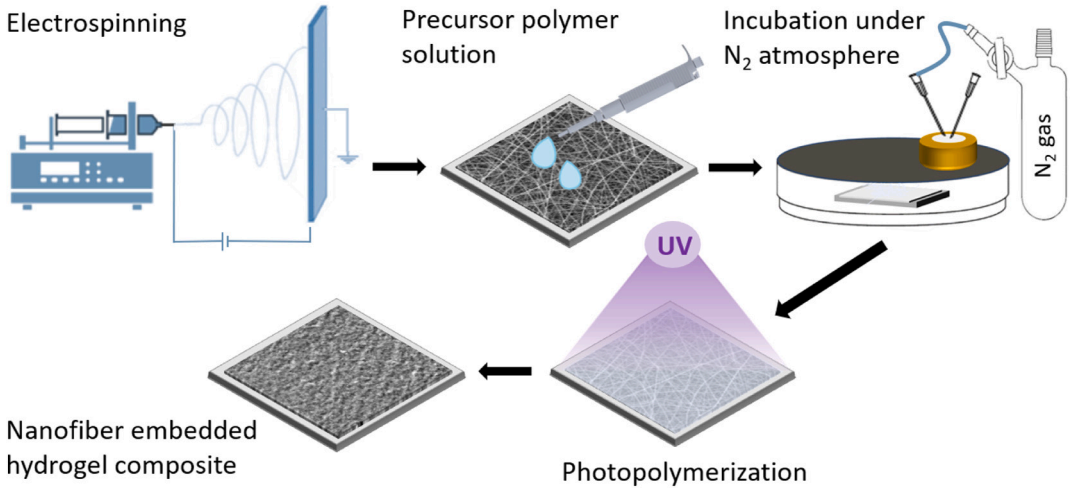

Fig. 1. Schematic representation of the sample preparation.

retained the biocompatibility and bioactivity properties of the gelatin, and thus, these properties have made the GelMA hydrogel one of the most studied soft materials for various medical applications such as drug/gene delivery and tissue engineering [13]. In the many former studies, GelMA hydrogels were used in cornea stroma engineering and promising results have been obtained in terms of high cell viability and transparency compared to natural corneal structure [8]. However, the main drawback of the GelMA hydrogel for the tissue engineering application is its weak mechanical property. This challenge can be improved by combining with an accompanying polymer to enhance the mechanical properties of GelMA hydrogels [14]. Therefore, poly(2-hydroxymethyl methacrylate) (p(HEMA)) hydrogels can be combined with GelMA using various methods [15,16]. p(HEMA) is a well-known hydrogel and has been widely used in the construction of various biomedical prostheses and is the first recommended hydrogel for keratoprosthesis [7]. It is hydrogel and stable against many chemical and biochemical reactions. Additionally, it is transparent and biocompatible material with a low cellular affinity [15,17]. Therefore, it has been used for the manufacturing of ophthalmic materials such as soft contact lenses and intraocular lenses [18].

Electrospinning has been actively used in many fields since the early 20th century [19]. It allows for the fabrication of fibers from micrometers to nanometers in km-long in one step without post-processing [20]. The ability to control morphology including fiber diameter, shape, and porosity by changing solution and process parameters make electrospinning a versatile process. The final properties of the fibers are determined by the solution parameters such as molecular weight and polymer properties, and also processing parameters such as electrical potential, orifice diameter, the distance between the collector and the polymer at the orifice, and flow rate at the syringe pump [21,22]. Electrospun fibers are quite suitable for biomedical and tissue engineering applications due to the high aspect ratio, high surface area, and flexibility [23]. Previous studies show that the fabrication of composite materials by the integration of electrospun fibers into the hydrogel matrix have been altered the mechanical property and widen the application area of the materials [24–27].

In the past, GelMA-p(HEMA) composite hydrogels were reported to be used in cornea and stroma of cornea engineering applications [15]. In this study, opaque GelMA fibers with sub-micron diameter were fabricated using the electrospinning method and embedded in p(HEMA) hydrogel as like the corneal stroma. Thus, the satisfactory and biocompatible properties of the GelMA fibers and p(HEMA) were combined for the development of a corneal engineering candidate material with improved transparency and sufficient mechanical properties. This promising combination and design of the composite hydrogels have not been reported up to now in the literature according to the best of our knowledge. To achieve this goal, the p(HEMA) and GelMA-p(HEMA) were prepared via UV initiated photo-polymerization in the presence of a photo-initiator. The biocompatibility and cell adhesion profiles were investigated using in vitro experiments. GelMA was used instead of collagen fibers and p(HEMA) was employed as a glue instead of glycoproteins to combine two different hydrogels in one body. As prepared composite hydrogels had appropriate mechanical strength for handling, high transparency, and biocompatibility. These findings indicated that the hydrogel materials would be a good candidate as an artificial stroma for anterior lamellar keratoplasty.

2. Materials and methods

2.1. Materials

Gelatin methacryloyl (GelMA, bloom 300, 80% degree of substitution), 1,1,1,3,3,3-hexafluoro-2-propanol (HFIP, ≥99%), 2-hydroxyethyl methacrylate (HEMA, 97%), 2-hydroxy-4′-(2-hydroxyethoxy)-2-methylpropiophenone (Irgacure 2959, 98%), *N*,*N*′-methylenebisacrylamide (MBA, ≥99.5%), phosphate buffered saline (PBS) tablet were purchased from Sigma Aldrich (St. Louis, MO, USA). Endothelial cell of *Bos taurus* cow cornea, BCE C/D-1b (ATCC® CRL-2048™), were purchased from ATCC. Human serum albumin, human immunoglobulins and lysozyme were supplied from Sigma-Aldrich and used as received. All other chemicals were of analytical rank and obtained from Merck KGaA, Darmstadt, Germany.

For cell culture studies; BCE C/D-1b corneal endothelial cell line (ATCC® CRL2048™), Dulbecco's modified Eagle's medium (DMEM), fetal bovine serum (FBS), phosphate buffer saline (PBS), sodium pyruvate, trypsin-EDTA from GIBCO (Grand Island, NY), and resazurin sodium salt, penicillin-streptomycin (P/S) from Sigma (St. Louis, MO) were used. Live/Dead™ Cell Viability Assay Kit was obtained from AAT Bioquest.

2.2. Optimization of electrospinning condition

In the fabrication of electrospun fibers, DC power supply (ES 40P, Gamma High Voltage Research) and syringe pump (NE-300, New Era Pump Systems, Inc.) were used. For the fabrication of submicron, homogeneous and bead-free fibers, various parameters such as the concentration of polymer and potential difference were examined. First, the effect of polymer concentration was investigated, to this, GelMA solutions were prepared by dissolving GelMA macro-monomer into HFIP at three different concentrations (i.e., 3, 5, and 10% *w/v*). The GelMA

solutions were stirred at room temperature continuously for 6.0 h before use. Electrospinning of the GelMA solutions at various concentration were realized by applying a constant potential difference of 11 kV, at 0.8 mL h^{-1} flow rate with a nozzle collector distance of 12 cm and at 23.6 °C under 50% humidity. Aluminum foil with a dimension of 13 × 11 cm^2 was used as a collector. The effect of voltage on the fiber properties was studied under the same experimental conditions (i.e., 11, 16, and 20 kV).

2.3. Preparation of p(HEMA) and GelMA-p(HEMA) hydrogels

Fabrication steps of samples were shown in Fig. 1. The prepolymer solution was prepared by mixing HEMA (as monomer), N,N methylene bisacrylamide (0.4% *w/v* of the amount of HEMA, as cross-linker) and Irgacure 2959 (10% w/v of the amount of HEMA, as a photoinitiator), the polymerization mixture was sonicated in ultrasonic bath for 15 min for homogenous distribution of the ingredients. Then, the solution was washed with nitrogen gas for 15 min for the removal of oxygen gas from the mixture. For the preparation of p(HEMA) samples, the prepolymer solution cast onto a polydimethylsiloxane (PDMS) mold, covered with a glass slide, and exposed to UV (365 nm) light for 10 min. The composite GelMA-p(HEMA) samples were prepared by adding 0.1 μL precursor polymer solution to the per mm^2 of membrane containing about 33 × 10^{-4} mg of fiber. For the production of the composite material, a 10 × 10 mm^2 fiber was placed in a flat glass petri dish, and a 10 μL of the polymerization solution was added over the GelMA fibers. The cover of the glass petri dish was modified with an inlet and outlet port for nitrogen gas. It was then covered with aluminum foil and nitrogen gas was purged approximately 15 min during incubating at the dark. After this period, photo-polymerization was realized by exposing the system to UV light (0.5 W/cm^2) at 365 nm a distance of 25 cm for 10 min.

2.4. Characterization of hydrogels

2.4.1. Morphology of fibers and hydrogels

Scanning electron microscopy (SEM, FEI Quanta 250 FEG, Oregon, US) was used for determination of the surface morphology of the electrospun GelMA fibers, GelMA-p(HEMA) composite and cross-section of materials. The samples were coated with a thin layer of gold then their surface was scanned by electron microscopy. To examine the cross-section of the composite material, the composite sample was immersed in liquid nitrogen for 1 min, and then broken to open the cross-sectional surface. Average fiber diameter was calculated from the SEM images using ImageJ software and analyzed by OriginPro 9.0 (OriginLab). The calculation was realized by measuring at least 100 representative fibers.

2.4.2. FT-IR study

Attenuated total reflectance Fourier-transform infrared (ATR-FTIR) spectra of the GelMA fibers, pure p(HEMA) and GelMA-p(HEMA) composite were studied with an ATR-FTIR spectrometer (Frontier MIR/FIR Spectrometer, PerkinElmer Inc., USA). The spectrum was obtained in a range of 600–4000 cm^{-1}.

2.4.3. Mechanical property of the hydrogels

Tensile properties (i.e. tensile strength, Young's modulus, and elongation at break) of p(HEMA) and GelMA-p(HEMA) hydrogels were determined by using a Texture Analyzer TA-XT2 (Stable Microsystem, Goldalming, UK) with a 5 kg load cell. The samples were stretched with a 0.5 mm s^{-1} crosshead speed until failure. Hydrogel films were prepared with PDMS mold into 8 × 50 mm^2 strips, then samples were incubated at 37 °C in PBS for 24 h. Before the testing samples were sprayed with distilled water to reduce the drying effect. The $n = 3$ was used in calculations of hydrogels' mechanical properties. It should be noted that tensile testing was performed using the automatic trigger mode of the texture analyzer. The probe of the device moves up until the strain gauge reaches the trigger force (0.049 N in our experiments), then the measurement starts. For this reason, the stress-strain curves obtained in our experiments start after the 0.049 N stress value is exceeded.

2.4.4. Transmittance of the hydrogels

The light transmittance of the composite material was measured by using UV–Vis spectrophotometer (DR 6000 Spectrophotometer, Hach, Colorado, US) by scanning at the visible light region at between 400 and 700 nm with a scanning interval of 5 nm. For each measurement, a 2.0 × 1.0 cm^2 strip sample was prepared for measurement. The sample was incubated at 37 °C in PBS solution for 24 h. After this period, the sample was placed on the wall of the spectrometer cuvette containing PBS solution and the transmittance was measured. The PBS solution was used as a blank in these measurements. The thickness of the p(HEMA) and GelMA-p(HEMA) sample is ~122 μm and ~74 μm, respectively; on the other hand, it is between 540 μm and 560 μm for the human cornea. It should be noted that the used samples thickness was not the same as that of the human cornea.

2.4.5. Swelling and water retention properties of the hydrogels

For the swelling test, the purified water (10 mL) was transferred into the centrifuge tube and the samples were placed into the centrifuge tube for 24 h. At the end of this period, the samples were removed from the centrifuge tube and the excess water of the samples was removed by adsorption with a filter paper. Then, it was weighted, and recorded as wet weight (W_w). To obtain the dry weight of the sample, they were dried in a freeze dryer (FreeZone 6 Liter Benchtop Freeze Dryer, Labconco, Kansas City, US). The samples were placed in 2 mL centrifuge tubes, covered with aluminum foil, perforated with a small stick, and placed in the freeze dryer. The dry weight (W_d) of the sample was weighed, and the percent swelling degree was calculated using the following formula:

$$\text{Degree of swelling } (\%) = [(W_w - W_d)/W_d] \times 100$$

The freeze-dried samples were transferred in phosphate buffer solution (PBS) and incubated in a water bath at 37 °C for 24 h. After that, the sample was weighed after removing of the excess water by absorption with a filter paper. Then the sample was left at room temperature (25.7 °C and 74% humidity) and weighted at predetermined time intervals (W_t). In the first 60 min, the samples were weighed at 5 min time intervals. Then, they were weighed up to 90 min with 10 min time intervals. The final weighs were obtained from the samples after 120 min incubation period. Percent of water retention was calculated by the following formula. Thus, a reduction in the weight of the samples over time was observed. All swelling and water retention analyzes were at least repeated with three similar samples.

$$\text{Water retention } (\%) = (W_t - W_d)/W_d \times 100$$

2.4.6. Contact angle and surface energy studies

Contact angles to water, glycerol and dimethyl sulfoxide of p(HEMA) and GelMA-p(HEMA) samples were measured by sessile drop method at 25 °C by using a digital optical contact angle meter Phoneix 150 (Surface Electro Optics, Korea). The measurements were the average of five contact angles at least operated on three membrane samples. The surface free energy parameters of as prepared samples were determined using the average contact angle value of the probe liquids. The results are evaluated using by the van Oss's acid-base method [28–30].

$$\gamma_l cos\theta = \gamma_s - \gamma_{sl}$$

where γ_l is the surface energy of the liquid, γ_{sl} is the interfacial energy of solid/liquid interface and γ_s is the surface energy of solid. The van Oss acid/base method is based on the contact angles against at least three test liquids with known values of γ^{LW}, γ^+ and γ^- are measured and the superscripts (^{LW}), ($^+$), and ($^-$) refers to dispersive Lifshitz-van der Waals and Lewis acid and base components, respectively. The obtained contact

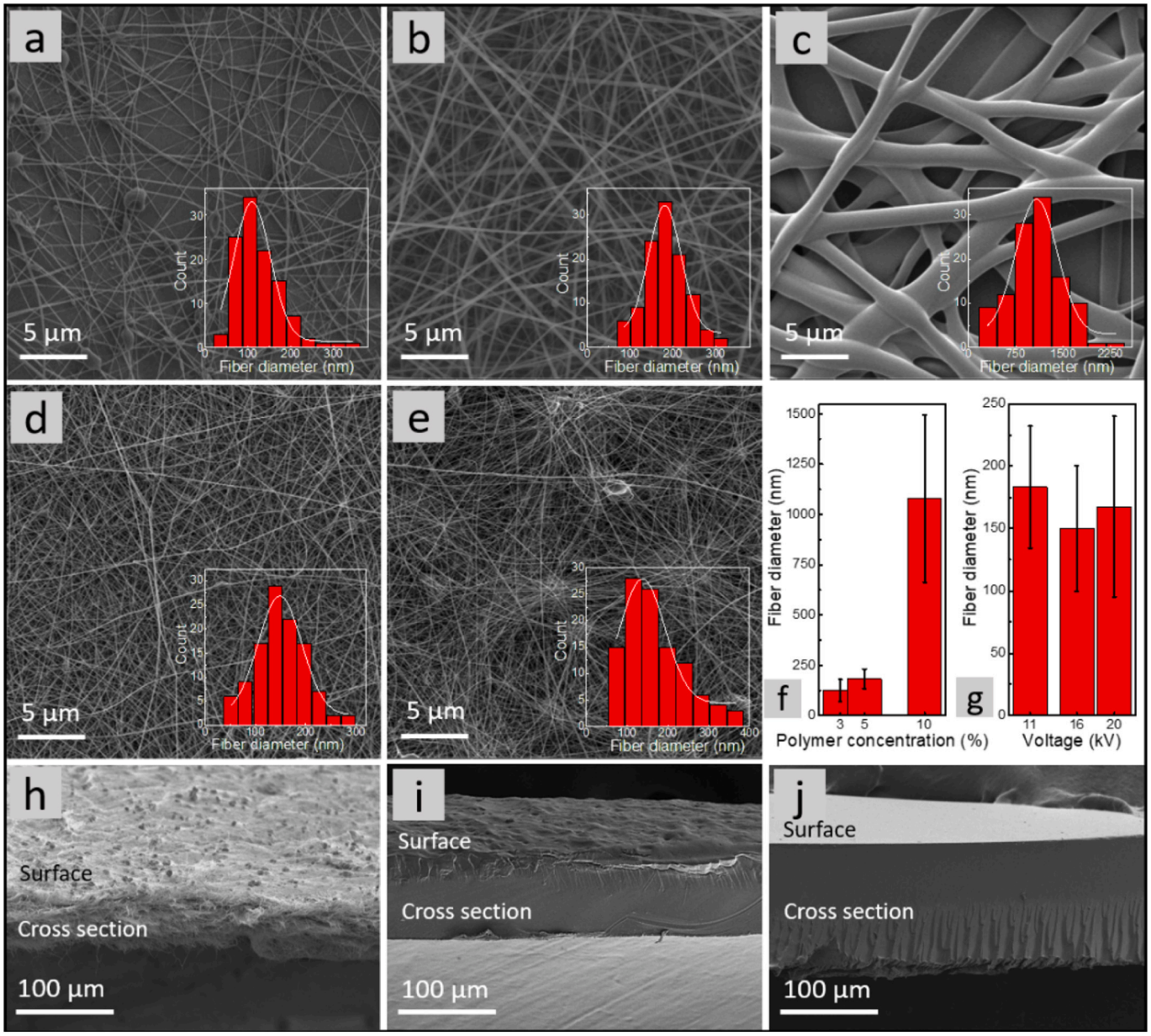

Fig. 2. SEM images the of electrospun fibers with various GelMA concentration at 11 kV: (a) 3%, (b) 5% and, (c) 10% *w/v*. Electrospun fibers at constant GelMA concentration (5% *w/v*) at various voltages: (d) 16 kV, and, (e) 20 kV. Graphs of (f) polymer concentration and (g) voltage versus fiber diameter. SEM images of cross section of fiber membrane electrospun at 16 kV with 5% w/v (h) GelMA, (i) GelMA-p(HEMA) composite film, and (j) p(HEMA) film.

angle values for each sample are place into the following equation:

$$\gamma_l(1+cos\theta) = \left(\gamma_s^{LW}\gamma_l^{LW}\right)^{1/2} + \left(\gamma_s^{+}\gamma_l^{-}\right)^{1/2} + \left(\gamma_s^{-}\gamma_l^{+}\right)^{1/2}$$

The total surface energy γ_s is regarded as the sum of Lifshitz-van der Waals and the Lewis acid and base components.

$$\gamma^{TOT} = \gamma^{LW} + \gamma^{AB}$$

where γ^{LW} designates Lifshitz-van der Waals interaction was calculated from the measured diiodomethane contact angles, and γ^{AB} designates such acid-base interactions as hydrogen bonding which is calculated from water and glycerol contact angles, and γ^{+} and γ^{-} refer to proton and electron donating character, respectively [31]. All the methods equations were solved using Phoenix 150 software.

2.4.7. Bio-compatibility studies

2.4.7.1. Interaction of hydrogels samples with tear fluid proteins. To determine the interaction of the p(HEMA) and GelMA-p(HEMA) with tear fluid proteins, the amount of adsorbed of human serum albumin (HSA), human immune-globulins (HIg), and lysozyme (LYZ) was studied at 37 °C for 12.0 h in PBS solution. The initial concentration of each protein was 0.1 mg/mL in the individual adsorption medium. The amount of adsorbed protein on the film surface was obtained by the following equation:

$$q = (C_0 - C)V/S$$

where q is the amount of protein adsorbed onto the sample surface (µg/cm^2); C_o and C are the initial and final concentrations of proteins in the solution (mg/mL), respectively. V is the volume of the protein solution; and S is the surface area of the sample. The amounts of laden protein

onto the p(HEMA) and GelMA-p(HEMA) were determined using Coomassie Brilliant Blue as described by Bradford [32]. Calibration curves were prepared from HSA, HIg, and LYZ and used in the calculation of the protein content of the solutions (0.01–0.2 mg/mL).

2.4.7.2. Hemolytic activity of hydrogel samples. Hemolysis is an important factor to assess the biocompatibility of a material [33]. Hence, hemolytic assays were performed to examine interaction of the hydrogel samples with red blood cell. The p(HEMA) and GelMA-p(HEMA) composite were used for the measuring of the released hemoglobin. Briefly, the fresh anticoagulated blood was obtained from Gazi University, Faculty of Medicine, Ankara, Turkey. The whole human blood was diluted with 1:1 ratio with PBS solution. The 0.5 mL diluted blood and 10 mL PBS solution were mixed with the tested samples. The positive controls consisted of 0.5 mL diluted blood with 10 mL distilled water, and the negative controls consisted 0.5 mL blood with 10 mL PBS solution. The samples were incubated at 37 °C for 60 min and the samples were removed from the test medium. Hemolytic activity was calculated by subtracting the absorbance of the negative control (PBS solution) and dividing by the absorbance caused by distilled water (positive control, 100%). As expected, complete hemolysis was observed in distilled water, which was the positive control but was negligible in PBS solution (negative control). The relative optical density compared to that of the red blood cells incubated in distilled water was defined as the percentage of hemolysis and the absorbance of the samples was measured at 570 nm.

2.4.7.3. 3D cell culture and toxicity studies. BCE C/D-1b corneal endothelial cells were cultured in DMEM medium supplemented with 10% FBS, 1% sodium pyruvate and 1% penicillin-streptomycin at 37 °C and 5% CO_2 and harvested when they reach to 80% confluency. For 3D cell culture studies, GelMA-p(HEMA) scaffolds were immersed in UP H_2O and then sterilized under UV prior to cell seeding. Sterilized scaffolds were conditioned overnight with DMEM medium supplemented with 10% FBS, 1% sodium pyruvate and 3% penicillin-streptomycin. After that, 1×10^5 BCE C/D-1b cells were seeded on conditioned scaffolds. As a control group, p(HEMA) hydrogel was used, and cells were cultured on it by using identical parameters.

To observe toxicity, cell proliferation and viability was analyzed via both AlamarBlue and Live/dead assays. Alamar Blue assay was conducted for long term at days 1, 3, 5 and 7. After cell culturing, scaffolds were incubated in DMEM, which contains 0.01% (*v*/v) resazurin sodium salt. After 4 h. of incubation, cell proliferation and viability profiles were analyzed through absorbance values at 570 and 600 nm. Quantitative viability analysis ($n = 3$) was done via OriginPro software (Northampton, MA). Live/Dead assay was done to visually determine the cellular viability and potential cytotoxic effects of GelMA-p(HEMA) scaffold on 3D cell culture. Equal volumes of Propidium Iodide and CytoCalcein were mixed in buffer solution and applied to the 3D cell cultured scaffolds with equal amount of DMEM. After 30 min. Incubation cells were observed under fluorescent microscope (Zeiss Observer Z1). Viability and image analysis were done by using Image J software (NIH).

2.5. Statistical analysis

All independent experiments were repeated at least three times under the same conditions. The statistical test was performed using one-way analysis of variance (ANOVA) on OriginPro 9 software. Significance level was set 0.05 and Tukey's method was used for the tests. At the 0.05 level, all the results obtained in the present work were not significantly different from the test mean.

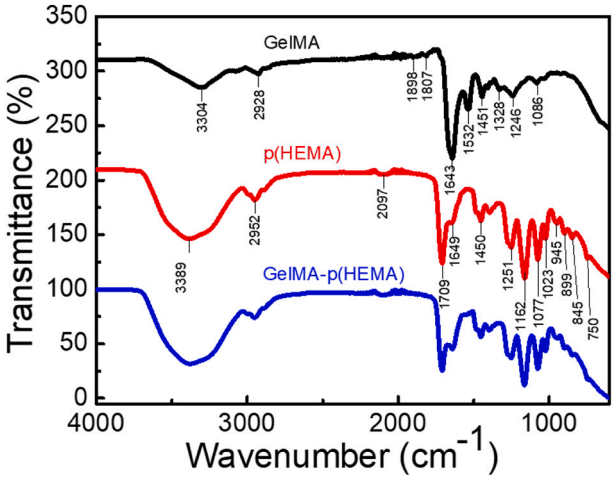

Fig. 3. FTIR spectra of GelMA fiber membrane, p(HEMA) and GelMA-p(HEMA).

3. Results and discussion

3.1. Morphology of fibers and hydrogels

Fig. 2 shows SEM images of the GelMA fibers, the diameter distributions of the fibers as inset, as well as the image of the cross-section of the GelMA-p(HEMA) fibrous composite. The fibers obtained from three different GelMA concentrations (i.e., 3, 5 and 10% *w/v*) are shown in Fig. 2a, b and c, respectively. The average diameter of the fibers produced from polymer solutions with a concentration of 3, 5 and 10% *w/v* were found 0.13 ± 0.6 μm, 0.18 ± 0.5 μm, and 1.08 ± 0.4 μm, respectively. Not surprisingly, the fibers become thicker as the polymer concentration increases (Fig. 2f). The fibers obtained from the solutions containing 3 and 5% w/v concentration were submicron size while the ones prepared from 10% w/v polymer were micrometer diameter. In addition, bead formation was observed in fibers of 3% GelMA concentration probably due to the existence of less entanglement, which is necessary for the formation of stable electospun jet and eventually continuous fibers. Fig. 2d and e show that the effect of potential difference on the fiber morphology. The average fiber diameter was found to be 0.15 ± 0.1 μm at 16 kV (spinning distance: 12 cm, fixed throughout the study) and 0.17 ± 0.1 μm at 20 kV. As seen in Fig. 2d, increasing the potential from 11 to 16 kV resulted in additional stretching of the fibers, and caused in the narrowing of the fiber diameter. However, increasing potential to 20 kV caused the fiber diameter distribution to widen and the cluster of the fibers in various regions (Fig. 2e). Fig. 2g shows that the fibers with 5% *w/v* polymer concentration at the voltage of 16 kV have the finest average fiber diameter with a low standard deviation. Therefore, the system was fixed at 5% w/v polymer solution and operated at 16 kV potential difference for further studies, and they were referred to as GelMA fiber. The SEM image of the GelMA fibers cross-section is presented in Fig. 2h. The thickness of the GelMA fiber membrane was found to be approximately 60 μm. Also, the cross-section and surface morphology of the GelMA-p(HEMA) composite material is shown in Fig. 2i. As prepared composite materials had rough surface morphology, and it could be due to the presence of the fibers in the composite structures. The approximate thickness of the composite material was measured as 74 μm. As observed in the cross-section of SEM image, the fibers appear to be homogeneously merged with prepolymer solution and embedded in the p(HEMA) matrix. Fig. 2j shows that the cross-section of p(HEMA) sample used in transmittance study with an approximate thickness of 122 μm, one of the thickest point of the composite.

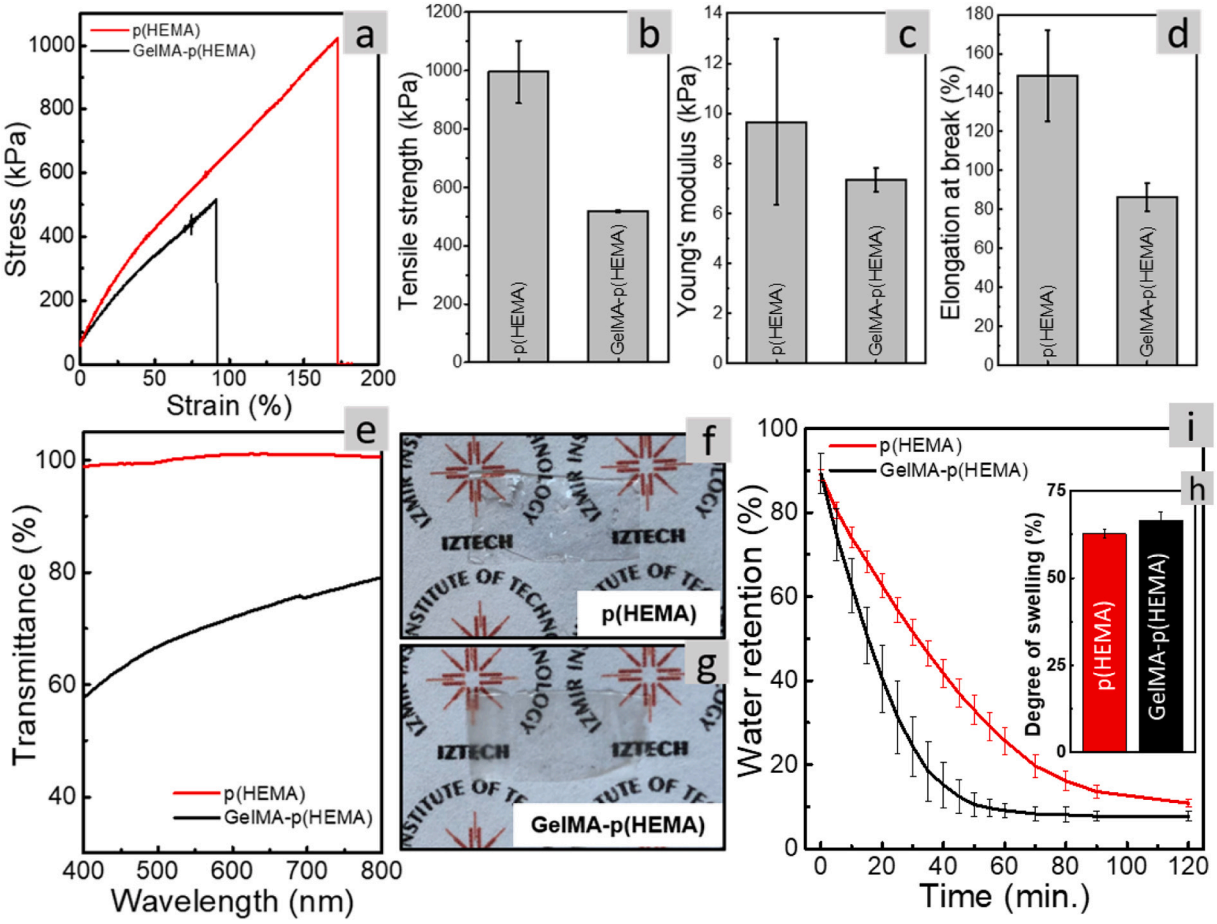

Fig. 4. Stress-strain curve (a), tensile strength (b), Young's modulus (c) and elongation at break (d) graphs of hydrogels. The transmittance (e) and photograph of the p(HEMA) (f) and GelMA-p(HEMA) (g) films. The degree of swelling (h) and time-varying water retention (i) of hydrogels.

3.2. FT-IR study

GelMA, p(HEMA) and GelMA-p(HEMA) were examined by ATR-FTIR spectrophotometer in the range of 600–4000 cm^{-1}. The spectra of the hydrogel samples are presented in Fig. 3. For the spectrum of the GelMA hydrogel, a broad stretching vibration band was observed at 3304 cm^{-1} and can be attributed to –OH groups of the gelatin units. The spectrum of gelatin is generally characterized by two remarkable vibrational bands (i.e., the amide I and the amide II band) at 1643 cm^{-1} and 1532 cm^{-1}. The former may be due to mainly to C═O stretching of the peptide groups of the gelatin, and the later band at 1532 cm^{-1} may result from –NH bending coupled with CN stretching, and this band is only observed in the protein structure. Additionally, N—H stretching band is observed at 3255 cm^{-1} overlapped with —OH groups band and can be attributed as amide A band. Moreover, the ATR-FTIR spectrum GelMA also showed absorption bands at 1451 and 1245 cm^{-1} and these bands were assigned in plane bending of $—CH_2$ groups in the GelMA structure. In addition, the band at 750 cm^{-1} is assigned as out of plane bending for ester groups (—C—O—) of p(HEMA). In the spectrum of p(HEMA), the —OH stretching vibration band was observed between approximately 3550 and 3300 cm^{-1}. This wide and intense band was centered at 3389 cm^{-1}. The antisymmetric stretching vibration band of methyl groups was observed at 2952 cm^{-1}, whereas the band at 1450 cm^{-1} is corresponding of -C-H stretching of the methyl groups. A strong band was observed in the spectrum of p(HEMA) at 1709 cm^{-1}. This was due to the stretching of free carbonyl group (C═O) in the ester functionality. Moreover, the characteristic absorption band of C—O was seen at 1251 cm^{-1}, and the antisymmetric stretching vibration band of C—O—C was assigned at 1162 cm^{-1}. For the GelMA-(HEMA), after combination of GelMA with HEMA broad stretching band of the –N–H and O—H bands were observed in the range of 2600–3600 cm^{-1}. Thus, the ATR-FTIR spectrum clearly indicated that p(HEMA) was present throughout the entire surface of GelMA fibers.

3.3. Mechanical property of the hydrogels

Biocompatible hydrogels should be mechanically durable enough to preserve their structure for implantation and compatible so as not to damage the surrounding tissue. The results of tensile properties of hydrogel samples are shown in Fig. 4a-d. Panel 4a displays the stress-strain curve of the materials. The tensile strength value of the p (HEMA) and GelMA-p(HEMA) were found to be 995 ± 107 kPa and 518 ± 1 kPa, respectively (Fig. 4b). The tensile strength of the GelMA-p (HEMA) composite was lower approximately half of the neat p(HEMA) hydrogel. Similar trends were also observed for Young's modulus (Fig. 4c) and elongation at break (Fig. 4d) graphs for the hydrogel samples. The p(HEMA) has 10 ± 3 kPa Young's modulus and withstand 149 ± 23% stretching whereas GelMA-p(HEMA) hydrogel have 7 ± 1 kPa Young's modulus and can withstand 86 ± 7% stretching. The calculations of the Young's modulus of the samples are shown in Fig. S1, S2 and S3. Methacrylate based polymers form hydrogen bonding between the polymer chains via carbonyl ester and hydroxyl groups. Thus, the hydrogen bonding interactions may led to increase in the stiffness of p (HEMA) compared to GelMA-p(HEMA) hydrogels [34,35]. On the other hand, GelMA is a modified protein with methacrylic acid anhydride, and has many large side groups on its amino acid residues. Therefore, the density of the polymer chains near the interface are expected to be lower. The large side groups of the amino acid residues may decrease the

hydrogen bond density and lead to lower adhesion energy. Our results are consistent with the literature. According to literature, the tensile strength of the synthesized GelMA-p(HEMA) composite hydrogel improved compared to the tensile strength of GelMA fibers (360 ± 40 kPa) reported in previous studies [36,37]. The Young's modulus of the GelMA-p(HEMA) composite (7 ± 1 kPa) is slightly lower than that of the natural human corneal modulus (10–570 × 10^2 kPa) [38,39]. The Young's modulus of collagen fibril, the directional orientation of fibrils, and the volume fraction of fibril are among the factors influencing Young's modulus along the corneal meridian [40]. Also, the modulus of the crosslinked GelMA fiber depends on the degree of substitution of methacrylic acid to the GelMA structure and the degree of crosslinking [36,37]. The random orientation of GelMA fibers and degree of crosslinking of the embedded GelMA in the p(HEMA) hydrogels could be responsible for the low elastic modulus of the proposed composite hydrogel [24,41,42].

3.4. Transmittance of the hydrogels

As shown in Fig. 4e and f, the structurally homogenous p(HEMA) hydrogel was observed to be optically transparent in visible light as expected [43]. The composite GelMA-p(HEMA) hydrogel transmits most of the light in the studied visible region (Fig. 4a and g), a part of the incident light is attenuated. The reason of attenuation (decreasing transmittance) may be due to the occurrence of rigorous optical scattering. Since the fiber and matrix have refractive index mismatch, optical scattering takes place. It was observed that the transmittance varies depending on the wavelength and increased from 58% to 74% in the studied range (400–800 nm). In this regard, the transmittance trend of GelMA-p(HEMA) composite resembles that of the human cornea [44], but still needs to be improved to get complete optical clarity.

3.5. Swelling and water retention properties of the hydrogels

The p(HEMA) is classified as moderately or poorly swollen hydrogels, and the degree of swelling may vary depending on the degree of crosslinking and type of crosslinker [45]. GelMA has a high degree of swelling ratio and this value decreases as the degree of substitution increases [46,47]. The degree of substitution of GelMA used in this study is 80%. Fig. 4h shows the average degree of the swelling ratios of the hydrogels. They were found to be 63% ± 1 for p(HEMA) and 66% ± 2 for GelMA-p(HEMA). The degree of swelling ratio of the p(HEMA) increased slightly with the inclusion of the GelMA electrospun fibers. The study of water retention capacity was performed between 0 and 120 min and the results are shown in Fig. 4i. The p(HEMA) reached equilibrium water retention within 2 h with slower deswelling rate, while GelMA-p(HEMA) reached within 1 h. It was observed that the initial water retention capacity of p(HEMA) and GelMA-p(HEMA) decreased by approximately 78% and 81% and reached equilibrium water retention values of 10% and 8% (at room temperature and at 74% humidity), respectively. These results indicate low retention capacity for both hydrogels.

3.6. Contact angle and surface energy studies

The contact angle data of the materials have been used to estimate the surface feature of the materials. The contact angle values of the test liquids were measured by putting a sessile drop of test liquid on the surface of the materials [33]. The materials surfaces can have various functional groups (such as —OH, —NH_2, —NH, —COOH, —CH_2, —CH_3, —SO_3H, —PO_4H_2 and aromatic molecules) for ionic, polar and hydrophobic interactions with biological macromolecules and cells. These physiological groups are highly important for the improving of biomaterials in the area of tissue engineering and regenerative medicine. The wettability of a material surface can be investigated by measuring the contact angles for water and diiodomethane since these two solvents are often used as reference liquids in analyses of interaction of polar and apolar liquids with solid material surface. In the present study, three different test liquids (i.e., purified water, glycerol and diiodomethane) were used to measure contact angle values of p(HEMA) and GelMA-p(HEMA) hydrogels. According to the Young equation, the smaller the surface tension of the test liquid, the smaller becomes the contact angle measured on the surfaces of samples. The data provide relatively different contact angle values depending on the occurrence of functional groups on the hydrogel materials. The contact angle value of a test material with a polar liquid is expected to be higher for a hydrophobic surface bed wetting or vice versa. As presented in Table 1, the highest contact angle values of the hydrogels were achieved with water, whereas diiodomethane yield the lowest contact angles. Both hydrogel samples were in hydrophilic nature and the water contact angles values p(HEMA) and GelMA-p(HEMA) were found to be 55.3 ± 0.8 and 40.3 ± 1.6, respectively. The GelMA-p(HEMA) hydrogel surface was more hydrophilic compared to neat p(HEMA). Not surprisingly, the GelMA has many hydrophilic amino acid residues on its surface (such as histidine, arginine, lysine, aspartic acid, glutamic acid and hydroxyl-proline), and these amino acid residues create a polar surface. As earlier reported, the increased surface wettability of the biomaterial could increase the biocompatibility for interaction of cells, which may suggest that slightly hydrophilic surfaces are more desirable for many biomedical applications [33].

Table 1
Contact angle values of the p(HEMA) and GelMA-p(HEMA) hydrogels to various test liquids (i.e., water, glycerol, and diiodomethane).

Type of hydrogels	Contact angles (θ°) of test liquids with their surface tension (γ_l)		
	γ_l = 71.3 mN/m water	γ_l = 64.0 mN/m glycerol	γ_l = 50.8 mN/m diiodomethane
p(HEMA)	55.3 ± 0.8	53.4 ± 1.3	40.1 ± 2.1
GelMA-p (HEMA)	40.3 ± 1.6	37.9 ± 2.1	36.8 ± 1.2

Table 2
Surface free energy parameters (mN/m) of the p(HEMA) and GelMA-p(HEMA) hydrogels according to the van Oss et al. method.

Type of hydrogel	γ^{LW} (mN/m)	γ^{+} (mN/m)	γ^{-} (mN/m)	γ^{AB} (mN/m)	γ^{TOT} (mN/m)	Polarity (%)
p(HEMA)	39.48	0.49	4.51	4.81	44.27	10.9
GelMA-p (HEMA)	43.98	1.07	5.17	12.8	55.97	21.6

The surface energy parameters of the studied p(HEMA) and GelMA-p (HEMA) hydrogel were calculated from the measured contact angle values according to the van Oss method and presented in Table 2. The overall surface free energy (γ^{TOT}) containing of the sum of the Lifschitz–van der Waals (γ^{LW}) and the acid–base components (γ^{AB}) had different values for both the examined hydrogel samples. Both p(HEMA) and GelMA-p(HEMA) seem to exhibit "amphoteric" character. On the other hand, the basic parameters (−) of both hydrogels are significantly greater than those of the acidic parameter (+). Relatively, the high basic (−) component of the surface energy of the p(HEMA) should be caused by the electron ion pairs of oxygen atoms containing in such as hydroxyl and carbonyl functionality. Whereas GelMA-p(HEMA) has additional carboxyl groups functionality (from glutamic acid aspartic acid residue in the GelMA) compared to the neat p(HEMA), which is also effective in Lewis base sites [33]. On the other hand, GelMA-p(HEMA) has a larger acidic parameter compared to p(HEMA) due the presence of high percentage of arginine (15.4%) and lysine (4.5%) in the gelatin structure. Both amino acids have pendant amine functionality on their residues. Both studied hydrogel samples, displayed different acid–base components (γ^{AB}) of the surface energy (γ^{TOT}) due to different chemical structures of the hydrogel surfaces. As can be seen from Table 2,

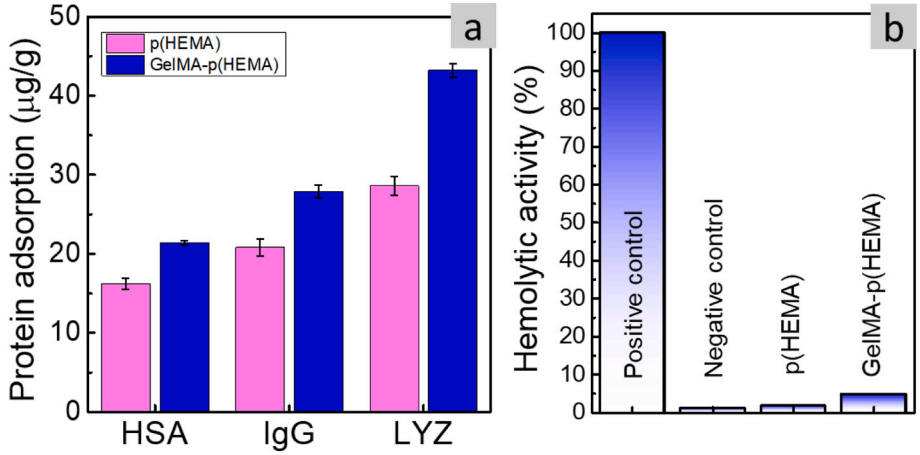

Fig. 5. Amount of protein adsorption (a) and hemolytic activity (b) of p(HEMA) and GelMA-p(HEMA) hydrogels.

hydroxyl, carbonyl, carboxyl, and amine groups functionality increase the polarity of the material, therefore, GelMA-p(HEMA) has a high polarity value (21.6%) in comparison to p(HEMA). As reported earlier, surface wettability is documented as a critical factor for interactions of protein and cell adhesion, and these biological macromolecules tend to attach better to slightly hydrophilic surfaces than to hydrophobic surfaces [48].

3.7. Bio-compatibility studies

3.7.1. Interaction of hydrogels samples with tear fluid proteins

Several studies have been focused to repair corneal tissue defect and collagen- and gelatin-based materials are being studied [11,49]. For corneal tissue replacement, the adsorption of protein on the designed materials should be avoided especially for the artificial cornea and corneal patches. The adsorption of proteins on a biomaterial, and then, the denaturation of adsorbed proteins can increase the probability of the attack of phagocytic and antigen-presenting cells. This can be led to tissue damage and implant fibrosis [49]. In addition, the adsorption of proteins on the surface of a biomaterial in a biological environment is the first step in the bacterial biofilm formation and play a part as a stimulator for additional bacterial adhesion. Therefore, the protein adsorption resistivity properties of GelMA-p(HEMA) network were tested with the major tear proteins was studied using the pure p(HEMA) as a control system. Human serum albumin (HSA; MW 66.4 kD,), immunoglobulin (IgG; MW 150 kD,) and lysozyme (LYZ; MW 14.4 kD) are the major tear fluid proteins. Therefore, they were selected as adsorbate proteins for the evaluation of the constructed composite hydrogel system and the major tear proteins interaction experiments were realized in a batch system. Each protein solution was prepared in physiological buffer solution (pH 7.4) at a concentration of 0.1 mg/mL and contacted with p(HEMA) and GelMA-p(HEMA) materials at 37 °C for 12 h. The maximum amount of protein adsorbed on both p(HEMA) and GelMA-p(HEMA) materials were reached approximately 6.0 h and not significantly changed after this contact period. It should be noted that at isoelectric point (pI) is the pH value at which a protein molecule carries no net electrical charge on its surface. The net surface charge of a protein molecule can be affected by the solution pH value and can become more positively or negatively charged. Moreover, protein molecules contain both acidic and basic amino acid residues on their surface functional groups. The isoelectric points of the HSA, IgG, and LYZ were 4.0, 6.5, and 11.2, respectively, and therefore, HSA and IgG have negative charges whereas LYZ has positive charges at pH 7.4. Thus, if the pH value of a medium is lower than that of the pI value of protein, then has positive charge and above pI value is vice-versa. The gelatin (type A) shows a pI value in the range of 6.0–9.5, therefore carries a net negative charge at pH 7.4. The GelMA-p(HEMA) surfaces exhibited significant increase in lysozyme adsorption with respect to p(HEMA) hydrogel. The reasonably basic component of the GelMA-p(HEMA) composite can generate an attractive force towards the positively charged lysozyme molecules. On the other hand, the adsorbed amounts of HSA and IgG on the GelMA-p(HEMA) were slightly increased compared to pure p (HEMA) hydrogel. The amounts of the adsorbed HSA, IgG, and LYZ on the p(HEMA) hydrogel were less than those of the GelMA-p(HEMA) (Fig. 5a). The amount of adsorbed proteins on the p(HEMA) and GelMA-p(HEMA) materials surface were found to be 16.2 ± 0.7 and 21.4 ± 0.3 for HSA, 20.8 ± 1.1 and 27.9 ± 0.8 for IgG, and 28.6 ± 1.2 and 43.2 ± 0.9 μg/g for lysozyme, from individually tested proteins, respectively. Amounts of adsorbed HSA were slightly lower on both hydrogel samples with respect to IgG and lysozyme and this can be due to the acidic properties of the HSA and it has a lowest pI value compared to IgG and LYZ. In addition, the amounts of adsorbed protein onto both hydrogels increased as the pI value of the test protein increased. In the presented work, the functional amino acid residues of the gelatin in the GelMA structure may be moved from the interior to the surface of the GelMA-p(HEMA) materials during polymerization protocols, thus, the gelation functional groups on the GelMA structures yielded an accessible adsorptive site. Similar observations have been reported in the earlier studies [50,51]. Adsorption of proteins on the composite hydrogel surface indicated that there were binding sites on the surface, and similarly, the cells could be interacted with these regions.

3.7.2. Hemolytic activity of hydrogel samples

Hemolysis of red blood cells is an important factor to assess the biocompatibility of a material. The rupture of red blood cells, called hemolysis, is accompanied by the release of hemoglobin. Thus, an amplified concentration of the free hemoglobin in the plasma is a direct indicator of the red blood cells destruction. Hence, the destruction of the red blood cells can lead to the reduced oxygen transport to tissues and organs in vivo and enlarged levels of the free hemoglobin could induce toxicity in the respective tissues [52]. The hemolytic activity of the p (HEMA) and GelMA-p(HEMA) hydrogels was studied in vitro via hemolysis tests. As estimated, whole hemolysis was detected in distilled water and used as a positive control. Physiological saline solution was used as a negative control. The percentage hemolysis values of the p (HEMA) and GelMA-p(HEMA) hydrogels were found to be 1.63 ± 0.04 and 4.57 ± 0.09%, respectively (Fig. 5b). The insertion of gelatin in the polymer structure was increased hemolytic activity approximately 2.8 folds. The GelMA-p(HEMA) surface has been decorated with several amino acid residues of the gelatin (such as arginine, histidine, lysine, glutamic acid and aspartic acid residues) and they could be electrostatically interacted with several biological macromolecules. These

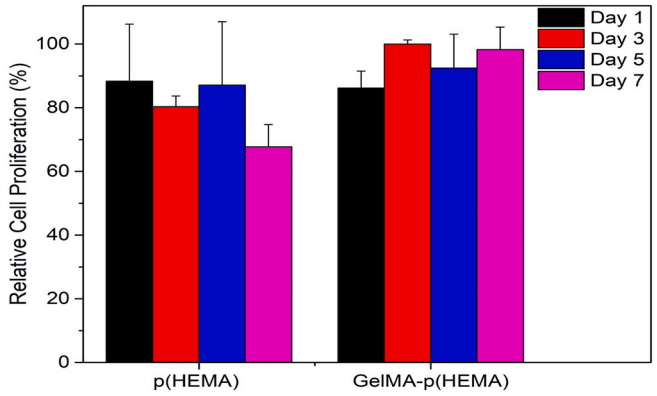

Fig. 6. Representative proliferation profiles of BCE C/D-1b cells on p(HEMA) and GelMA-p(HEMA) scaffold, evaluated by AlamarBlue assay for 1,3,5 and 7 days of culture ($n = 3$).

amino acid residues also permit ionic complex with the phospholipids of the red blood cells membrane and could be generate an imperfection mechanism. In this system, the amine group residue of the arginine and lysine could play a critical role in the GelMA-red blood cell surface interactions. In consistent with the literature, the polymers containing primary, tertiary or quaternary amine groups showed high hemolytic activity [53]. Thus, the hemolytic activity test result showed that the existence of functional amino groups increases the hemolytic activity of the material compared to p(HEMA). As stated earlier, up to 5.0% hemolysis is acceptable for the biomaterials [54]. Thus, the hemolysis activity of the GelMA-p(HEMA) was found to be 4.57 and could be used as appropriate hydrogel materials for numerous biomedical applications.

3.7.3. Cell viability and proliferation on GelMA-p(HEMA) scaffold

Biocompatibility of GelMA-p(HEMA) scaffolds was investigated to assess their potential as a scaffold for cornea tissue engineering. BCE C/D1b corneal endothelial cells were grown 3D on GelMA-p(HEMA) scaffolds to evaluate the cell proliferation and potential cytotoxic effects of GelMA-p(HEMA). Cell proliferation and viability was evaluated and quantified through both AlamarBlue (Fig. 6) and Live/dead assays (Fig. 7). BCE C/D-1b cells were adhered well on GelMA-p(HEMA) surface and showed high viability compared to the 3D control p(HEMA) group. The number of cells increased gradually during 1-week culturing, where p(HEMA) control group showed decreasing proliferation profile. Moreover, cell viability and proliferation were examined visually via Live/dead analysis as given in Fig. 7. The number of cells slowly increased up to day 3, which is expected due to slow cell adhesion and

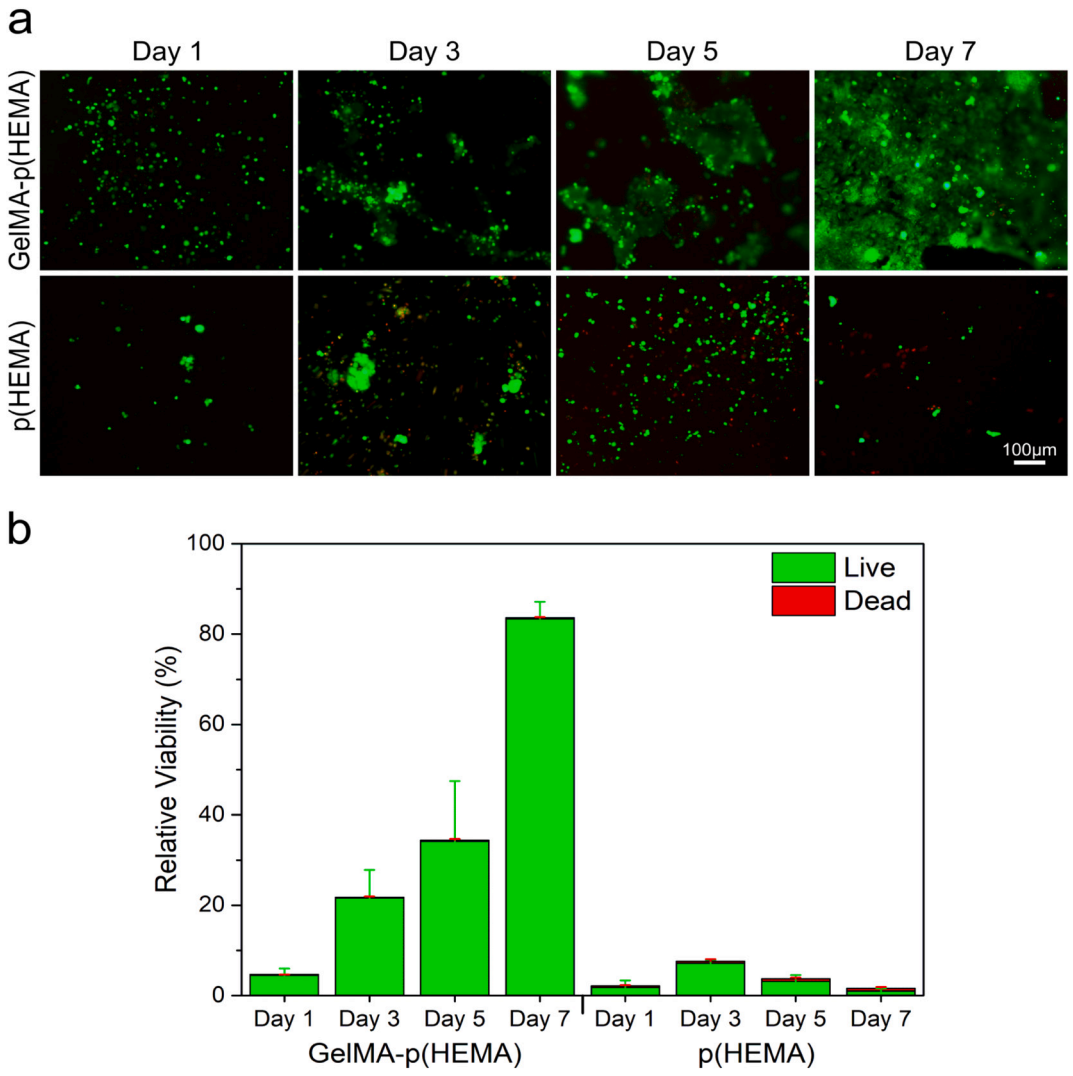

Fig. 7. (a) Live-dead assay, and (b) Cell viability profile of BCE C/D-1b cells on p(HEMA) and GelMA-p(HEMA) scaffold, for 1,3,5 and 7 days of culture (scale bar = 1 (Green: live cells, red: dead cell, $n = 3$). (For interpretation of the references to colour in this figure legend, the reader is referred to the web version of this article.)

adaptation in 3D microenvironment. In contrast to p(HEMA) control group, cell adaptation to GelMA-p(HEMA) scaffold started to increase from day 3 and higher proliferation rate was observed from day 3 onwards. This result can be explained as follows: GelMA-p(HEMA) scaffold provides a suitable 3D microenvironment, where cell-cell and cell-material interaction is favored. In addition, cell proliferation increases in long-term since fibrillar structure of GelMA-p(HEMA) provides more space and increased surface area compared to p(HEMA) hydrogel itself. Overall, BCE C/D-1b cells proliferated well within the GelMA-p(HEMA) scaffold, which indicates that GelMA-p(HEMA) scaffold is highly biocompatible and can be a suitable scaffold for cornea tissue engineering.

4. Conclusions

In this study, GelMA fibers were prepared via electrospinning, and surrounded with p(HEMA) matrix. The combination of the both components was subsequent1y polymerized in the presence of a photo-initiator using UV photo-polymerization. The synthesized GelMA-p(HEMA) composite was characterized physical, mechanical, and biological methods using pure p(HEMA) hydrogel as a control system. The optical transmittance trend of the composite material in visible light was similar to that of the human cornea and it was promising for the future use in the intended corneal repairing. For future application, the neat GelMA was not sufficient in terms of mechanical properties and not even hand able for the characterization of the material. Therefore, the combination of p(HEMA) with GelMA notably improved mechanical property of neat GelMA and also made to be strong enough to withstand handling. Additionally, the GelMA-p(HEMA) hydrogel was also tested to observe the structural integrity of the composite hydrogel for desired incubation periods to provide as a mechanical scaffold for 3D corneal cell culture. For this purpose, the BCE C/D¬1b corneal endothelial cells were cultured in 3D on the GelMA-p(HEMA) hydrogels. The results demonstrated that the cultured cells were proliferating well after adaptation period, which is day 3, and any potential cytotoxic effect was not observed. Adsorption and growth profile of BCE C/D¬1b corneal endothelial cells on GelMA-p(HEMA) hydrogels showed promise for biomedical applications where easy and inexpensive production could be of paramount importance. Finally, the GelMA-p(HEMA) composite hydrogels showed highly promising mechanical property, optical transmittance in visible light (from 58 to 74% at 400–500 nm) and improved biological performance. Thus, GelMA-p(HEMA) hydrogels could have a good candidate due to promising properties as a scaffold in tissue engineering particularly for corneal applications.

CRediT authorship contribution statement

Tugce A. Arica: Conceptualization, Investigation, Methodology, Writing - original draft, Formal analysis. **Meltem Guzelgulgen:** Investigation, Formal analysis. **Ahu Arslan Yildiz:** Supervision, Writing - review & editing. **Mustafa M. Demir:** Supervision, Project administration, Validation, Writing - review & editing.

Declaration of competing interest

The authors declare that they have no known competing financial interests or personal relationships that could have appeared to influence the work reported in this paper.

Acknowledgement

This work was supported by the Izmir Institute of Technology Scientific Research Project [grant number IYTE 0322]. Freeze drying and microscopy studies were carried out at the Izmir Institute of Technology Biotechnology and Bioengineering Application and Research Center and Materials Research Center, respectively. The authors thank Prof. Dr. M. Yakup Arica for contact angle measurements and fruitful discussions.

Appendix A. Supplementary data

Supplementary data to this article can be found online at https://doi.org/10.1016/j.msec.2020.111720.

References

[1] K.M. Meek, C. Knupp, Corneal structure and transparency, Prog. Retin. Eye Res. 49 (2015) 1–16, https://doi.org/10.1016/j.preteyeres.2015.07.001.
[2] M. Sridhar, Anatomy of cornea and ocular surface, Indian J. Ophthalmol. 66 (2018) 190–194, https://doi.org/10.4103/ijo.IJO_646_17.
[3] D.M. Maurice, The structure and transparency of the cornea, J. Physiol. 136 (2) (1957) 263, https://doi.org/10.1113/jphysiol.1957.sp005758.
[4] J. Xiang, J. Sun, J. Hong, W. Wang, A. Wei, Q. Le, J. Xu, T-style keratoprosthesis based on surface-modified poly (2-hydroxyethyl methacrylate) hydrogel for cornea repairs, Mater. Sci. Eng. C 50 (2015) 274–285, https://doi.org/10.1016/j.msec.2015.01.089.
[5] P. Gain, R. Jullienne, Z. He, M. Aldossary, S. Acquart, F. Cognasse, G. Thuret, Global survey of corneal transplantation and eye banking, JAMA Ophthalmology 134 (2) (2016) 167–173, https://doi.org/10.1001/jamaophthalmol.2015.4776.
[6] B. Kong, S. Mi, Electrospun scaffolds for corneal tissue engineering: a review, Materials 9 (8) (2016) 614, https://doi.org/10.3390/ma9080614.
[7] D. Myung, P.E. Duhamel, J.R. Cochran, J. Noolandi, C.N. Ta, C.W. Frank, Development of hydrogel-based keratoprostheses: a materials perspective, Biotechnol. Prog. 24 (3) (2008) 735–741, https://doi.org/10.1021/bp070476n.
[8] S. Matthyssen, B. Van den Bogerd, S.N. Dhubhghaill, C. Koppen, N. Zakaria, Corneal regeneration: a review of stromal replacements, Acta Biomater. 69 (2018) 31–41, https://doi.org/10.1016/j.actbio.2018.01.023.
[9] J.Y. Li, M.A. Greiner, J.D. Brandt, M.C. Lim, M.J. Mannis, Long-term complications associated with glaucoma drainage devices and Boston keratoprosthesis, Am J. Ophthalmol. 152 (2) (2011) 209–218, https://doi.org/10.1016/j.ajo.2011.07.014.
[10] E.K. Akpek, M. Alkharashi, F.S. Hwang, S.M. Ng, K. Lindsley, Artificial Corneas Versus Donor Corneas for Repeat Corneal Transplants, Cochrane Database of Systematic Reviews (11), 2014, https://doi.org/10.1002/14651858.CD009561.pub2.
[11] Ahearne M., Fernández-Pérez J., Masterton S., Madden P.W., Bhattacharjee P., Designing Scaffolds for Corneal Regeneration, Advanced Functional Materials n/a (n/a) 1908996, doi:10.1002/adfm.201908996.
[12] M. Sun, X. Sun, Z. Wang, S. Guo, G. Yu, H. Yang, Synthesis and properties of gelatin methacryloyl (GelMA) hydrogels and their recent applications in load-bearing tissue, Polymers 10 (11) (2018) 1290, https://doi.org/10.3390/polym10111290.
[13] K. Yue, G. Trujillo-de Santiago, M.M. Alvarez, A. Tamayol, N. Annabi, A.J. B. Khademhosseini, Synthesis, properties, and biomedical applications of gelatin methacryloyl (GelMA) hydrogels 73 (2015) 254–271, https://doi.org/10.1016/j.biomaterials.2015.08.045.
[14] L. Elomaa, E. Keshi, I.M. Sauer, M. Weinhart, Development of GelMA/PCL and dECM/PCL resins for 3D printing of acellular in vitro tissue scaffolds by stereolithography, Mater. Sci. Eng. C 112 (2020) 110958, https://doi.org/10.1016/j.msec.2020.110958.
[15] L. Wang, C. Lu, H. Liu, S. Lin, K. Nan, H. Chen, L. Li, A double network strategy to improve epithelization of a poly(2-hydroxyethyl methacrylate) hydrogel for corneal repair application, RSC Adv. 6 (2) (2016) 1194–1202, https://doi.org/10.1039/C5RA17726J.
[16] D.-M. Dragusin, S. Van Vlierberghe, P. Dubruel, M. Dierick, L. Van Hoorebeke, H. A. Declercq, M.M. Cornelissen, I.-C. Stancu, Novel gelatin–PHEMA porous scaffolds for tissue engineering applications, Soft Matter 8 (37) (2012) 9589–9602, https://doi.org/10.1039/C2SM25536G.
[17] M.F. Passos, D.R.C. Dias, G.N.T. Bastos, A.L. Jardini, A.C.B. Benatti, C.G.B.T. Dias, R. Maciel Filho, pHEMA hydrogels, J. Therm. Anal. Calorim. 125 (1) (2016) 361–368, https://doi.org/10.1007/s10973-016-5329-6.
[18] X. Hu, L. Hao, H. Wang, X. Yang, G. Zhang, G. Wang, X. Zhang, Hydrogel contact lens for extended delivery of ophthalmic drugs, International Journal of Polymer Science 2011 (2011), https://doi.org/10.1155/2011/814163.
[19] J. Doshi, D.H. Reneker, Electrospinning process and applications of electrospun fibers, J. Electrost. 35 (2) (1995) 151–160, https://doi.org/10.1016/0304-3886(95)00041-8.
[20] A. Greiner, J.H. Wendorff, Electrospinning: a fascinating method for the preparation of ultrathin fibers, Angew. Chem. Int. Ed. 46 (30) (2007) 5670–5703, https://doi.org/10.1002/anie.200604646.
[21] M.M. Demir, Investigation on glassy skin formation of porous polystyrene fibers electrospun from DMF, EXPRESS Polym. Lett. 4 (1) (2010) 2–8, https://doi.org/10.3144/expresspolymlett.2010.2.
[22] M.M. Demir, I. Yilgor, E. Yilgor, B. Erman, Electrospinning of polyurethane fibers, Polymer 43 (11) (2002) 3303–3309, https://doi.org/10.1016/S0032-3861(02)00136-2.
[23] A. Hasan, A. Memic, N. Annabi, M. Hossain, A. Paul, M.R. Dokmeci, F. Dehghani, A. Khademhosseini, Electrospun scaffolds for tissue engineering of vascular grafts, Acta Biomater. 10 (1) (2014) 11–25, https://doi.org/10.1016/j.actbio.2013.08.022.
[24] K. Tonsomboon, M.L. Oyen, Composite electrospun gelatin fiber-alginate gel scaffolds for mechanically robust tissue engineered cornea, J. Mech. Behav.

Biomed. Mater. 21 (2013) 185–194, https://doi.org/10.1016/j.jmbbm.2013.03.001.
[25] S. Xu, L. Deng, J. Zhang, L. Yin, A. Dong, Composites of electrospun-fibers and hydrogels: a potential solution to current challenges in biological and biomedical field, J. Biomed. Mater. Res. B Appl. Biomater. 104 (3) (2016) 640–656, https://doi.org/10.1002/jbm.b.33420.
[26] J.M. Shapiro, M.L. Oyen, Hydrogel composite materials for tissue engineering scaffolds, Jom 65 (4) (2013) 505–516, https://doi.org/10.1007/s11837-013-0575-6.
[27] M. Eslami, N.E. Vrana, P. Zorlutuna, S. Sant, S. Jung, N. Masoumi, R.A. Khavari-Nejad, G. Javadi, A. Khademhosseini, Fiber-reinforced hydrogel scaffolds for heart valve tissue engineering, J. Biomater. Appl. 29 (3) (2014) 399–410, https://doi.org/10.1177/0885328214530589.
[28] C.J. van Oss, Long-range and short-range mechanisms of hydrophobic attraction and hydrophilic repulsion in specific and aspecific interactions, J. Mol. Recognit. 16 (4) (2003) 177–190, https://doi.org/10.1002/jmr.618.
[29] W.A. Zisman, Relation of the Equilibrium Contact Angle to Liquid and Solid Constitution, Contact Angle, Wettability, and Adhesion, American Chemical Society, 1964, pp. 1–51, https://doi.org/10.1021/ba-1964-0043.ch001.
[30] F.M. Fowkes, Role of acid-base interfacial bonding in adhesion, J. Adhes. Sci. Technol. 1 (1) (1987) 7–27, https://doi.org/10.1163/156856187X00049.
[31] C.J. van Oss, M.K. Chaudhury, R.J. Good, Monopolar surfaces, Adv. Colloid Interf. Sci. 28 (1987) 35–64, https://doi.org/10.1016/0001-8686(87)80008-8.
[32] M.M. Bradford, A rapid and sensitive method for the quantitation of microgram quantities of protein utilizing the principle of protein-dye binding, Anal. Biochem. 72 (1–2) (1976) 248–254, https://doi.org/10.1016/0003-2697(76)90527-3.
[33] G. Bayramoglu, V. Bitirim, Y. Tunali, M.Y. Arica, K.C. Akcali, Poly (hydroxyethyl methacrylate-glycidyl methacrylate) films modified with different functional groups: in vitro interactions with platelets and rat stem cells, Mater. Sci. Eng. C 33 (2) (2013) 801–810, https://doi.org/10.1016/j.msec.2012.11.004.
[34] J.P.M. Lommerse, S.L. Price, R. Taylor, Hydrogen bonding of carbonyl, ether, and ester oxygen atoms with alkanol hydroxyl groups, J. Comput. Chem. 18 (6) (1997) 757–774, https://doi.org/10.1002/(sici)1096-987x(19970430)18:6<757::Aid-jcc3>3.0.Co;2-r.
[35] M.T. Lemon, M.S. Jones, J.W. Stansbury, Hydrogen bonding interactions in methacrylate monomers and polymers, J. Biomed. Mater. Res. A 83A (3) (2007) 734–746, https://doi.org/10.1002/jbm.a.31448.
[36] X. Zhao, X. Sun, L. Yildirimer, Q. Lang, Z.Y. Lin, R. Zheng, Y. Zhang, W. Cui, N. Annabi, A. Khademhosseini, Cell infiltrative hydrogel fibrous scaffolds for accelerated wound healing, Acta Biomater. 49 (2017) 66–77, https://doi.org/10.1016/j.actbio.2016.11.017.
[37] C. Chen, J. Tang, Y. Gu, L. Liu, X. Liu, L. Deng, C. Martins, B. Sarmento, W. Cui, L. Chen, Bioinspired hydrogel electrospun fibers for spinal cord regeneration, Adv. Funct. Mater. 29 (4) (2019) 1806899, https://doi.org/10.1002/adfm.201806899.
[38] A. Elsheikh, D. Wang, D. Pye, Determination of the modulus of elasticity of the human cornea, J. Refract. Surg. 23 (8) (2007) 808–818, https://doi.org/10.3928/1081-597X-20071001-11.
[39] K.E. Hamilton, D.C. Pye, Young's modulus in normal corneas and the effect on applanation tonometry, Optom. Vis. Sci. 85 (6) (2008) 445–450, https://doi.org/10.1097/OPX.0b013e3181783a70.
[40] C. Boote, S. Dennis, Y. Huang, A.J. Quantock, K.M. Meek, Lamellar orientation in human cornea in relation to mechanical properties, J. Struct. Biol. 149 (1) (2005) 1–6, https://doi.org/10.1016/j.jsb.2004.08.009.
[41] K. Tonsomboon, A.L. Butcher, M.L. Oyen, Strong and tough nanofibrous hydrogel composites based on biomimetic principles, Mater. Sci. Eng. C 72 (2017) 220–227, https://doi.org/10.1016/j.msec.2016.11.025.
[42] K. Tonsomboon, C.T. Koh, M.L. Oyen, Time-dependent fracture toughness of cornea, J. Mech. Behav. Biomed. Mater. 34 (2014) 116–123, https://doi.org/10.1016/j.jmbbm.2014.01.015.
[43] S. Vijayasekaran, T.V. Chirila, T.A. Robertson, X. Lou, J.H. Fitton, C.R. Hicks, I. J. Constable, Calcification of poly (2-hydroxyethyl methacrylate) hydrogel sponges implanted in the rabbit cornea: a 3-month study, J. Biomater. Sci. Polym. Ed. 11 (6) (2000) 599–615, https://doi.org/10.1163/156856200743896.
[44] E.M. Beems, J.A. Van Best, Light transmission of the cornea in whole human eyes, Exp. Eye Res. 50 (4) (1990) 393–395, https://doi.org/10.1016/0014-4835(90)90140-P.
[45] G. Mabilleau, I. Stancu, T. Honore, G. Legeay, C. Cincu, M. Basle, D. Chappard, Effects of the length of crosslink chain on poly (2-hydroxyethyl methacrylate) (pHEMA) swelling and biomechanical properties, Journal of Biomedical Materials Research Part A: An Official Journal of The Society for Biomaterials, The Japanese Society for Biomaterials, and The Australian Society for Biomaterials and the Korean Society for Biomaterials 77 (1) (2006) 35–42, https://doi.org/10.1002/jbm.a.30618.
[46] J.W. Nichol, S.T. Koshy, H. Bae, C.M. Hwang, S. Yamanlar, A. Khademhosseini, Cell-laden microengineered gelatin methacrylate hydrogels, Biomaterials 31 (21) (2010) 5536–5544, https://doi.org/10.1016/j.biomaterials.2010.03.064.
[47] M. Rizwan, G.S.L. Peh, H.-P. Ang, N.C. Lwin, K. Adnan, J.S. Mehta, W.S. Tan, E.K. F. Yim, Sequentially-crosslinked bioactive hydrogels as nano-patterned substrates with customizable stiffness and degradation for corneal tissue engineering applications, Biomaterials 120 (2017) 139–154, https://doi.org/10.1016/j.biomaterials.2016.12.026.
[48] K.L. Menzies, L. Jones, The impact of contact angle on the biocompatibility of biomaterials, Optom. Vis. Sci. 87 (6) (2010) 387–399, https://doi.org/10.1097/opx.0b013e3181da863e.
[49] H. Goodarzi, K. Jadidi, S. Pourmotabed, E. Sharifi, H. Aghamollaei, Preparation and in vitro characterization of cross-linked collagen–gelatin hydrogel using EDC/NHS for corneal tissue engineering applications, Int. J. Biol. Macromol. 126 (2019) 620–632, https://doi.org/10.1016/j.ijbiomac.2018.12.125.
[50] L. Liu, X. Li, X. Shi, Y. Wang, Injectable alendronate-functionalized GelMA hydrogels for mineralization and osteogenesis, RSC Adv. 8 (40) (2018) 22764–22776, https://doi.org/10.1039/C8RA03550D.
[51] M.M.M. De Paula, N.J. Bassous, S. Afewerki, S.V. Harb, P. Ghannadian, F. R. Marciano, B.C. Viana, C.R. Tim, T.J. Webster, A.O. Lobo, Understanding the impact of crosslinked PCL/PEG/GelMA electrospun nanofibers on bactericidal activity, PLoS One 13 (12) (2018), e0209386, https://doi.org/10.1371/journal.pone.0209386.
[52] S. Henkelman, G. Rakhorst, J. Blanton, W. van Oeveren, Standardization of incubation conditions for hemolysis testing of biomaterials, Mater. Sci. Eng. C 29 (5) (2009) 1650–1654, https://doi.org/10.1016/j.msec.2009.01.002.
[53] E.F. Palermo, K. Kuroda, Chemical structure of cationic groups in amphiphilic polymethacrylates modulates the antimicrobial and hemolytic activities, Biomacromolecules 10 (6) (2009) 1416–1428, https://doi.org/10.1021/bm900044x.
[54] R. Kronenthal, Polymers in mediCine and Surgery, Springer Science & Business Media, 2013, https://doi.org/10.1007/978-1-4684-7744-3.